Journal of Ceramic Processing Research. Vol. 19, No. 6, pp. 450~454 (2018)

J O U R N A L O F
Ceramic Processing Research

Microstructure control and change in thermal conductivity of 8YSZ/SiO_2 multi-compositional coating by suspension plasma spraying

Hak-Beom Jeon[a,b], In-Hwan Lee[b], Gye Seok An[a] and Yoon-Suk Oh[a,*]

[a]*Engineering Ceramic Center, Korea Institute of Ceramic Engineering & Technology, 3321 Gyeongchung-daero, Sindun-myeon, Icheon 467-843, Korea*

[b]*Department of Materials Science and Engineering Korea University, 145 Anam-ro, Seongbuk-gu, Seoul, Korea*

In recent years, thermal insulation coating technology for automotive engine parts has received significant attention as a means of improving the thermal efficiency of automotive engines. One of the characteristics of thermal insulation coatings is their low thermal conductivity, and, materials such as YSZ (Yttria-stabilized zirconia), which have low thermal conductivity, are used for this purpose. This research presents a study of the changes in the microstructure and thermal conductivity of 8YSZ/SiO_2 multi compositional thermal insulation coating for different compositions, and particle size distributions of suspension, when it is subjected to suspension plasma spraying. To obtain a porous coating structure, the mixing ratio of 8YSZ and SiO_2 particles and the particle sizes of the SiO_2 were changed. The microstructure, phase formation behavior, porosity and thermal conductivity of the coatings were analyzed. The porosities were found to be 1.2-32.1%, and the thermal conductivities of the coatings were 0.797-0.369 W/mK. The results of the study showed that the microstructures of the coatings were strongly influenced by the particle size distributions, and that the thermal conductivities of the coatings were greatly impacted by the microstructures of the coatings.

Key words: Thermal insulation coating, Suspension plasma spraying, Microstructure, Thermal conductivity, Porosity.

Introduction

Insulation coatings applied to the automotive engine combustion chambers or the components of turbine engines used for aerospace or power plants, which are exposed to high temperature environments, have been reported to enhance insulation and thermal durability [1-5]. Automotive engines, which have four strokes of intake, compression, combustion, and exhaust, generally exhibit higher energy efficiency when the combustion temperature is higher [6-8]. However, because the highest temperature of any point on piston should not exceed 66% of the melting point temperature of the alloy, it is difficult in raise the combustion temperature [9]. Extensive research has been conducted on achieving higher combustion temperatures and improving thermal efficiency using insulation coating technologies [10-12]. By coating the engine combustion chamber with insulation, insulation coatings control the thermal properties of the components comprising the combustion chamber, and, thus, minimize heat loss and enhance fuel economy.

The insulation coating of an engine piston needs to have a low thermal conductivity so that the gas temperature within the combustion chamber does not transfer to the surface of the combustion chamber wall. To obtain low thermal conductivity in the engine piston, previous studies have been carried out on fabricating porous coatings using materials, such as YSZ which have low thermal conductivities at high temperatures [13-16]. Especially, 8YSZ (8 mol% Yttria stabilized zirconia) is an ideal candidate material for thermal barrier coatings because it has good thermal shock resistance, high thermal stability, low density, and low thermal conductivity [17].

There are several methods for fabricating insulation coatings, the most prevalent of which, is the atmosphere plasma spray (APS) method [18-19]. APS produces a low thermal conductivity coating by spraying a layered structure. However, the fabricated APS coating has the disadvantage of embodying fractures in the layered structure parallel to the substrate surface, which reduce thermal durability [18-19]. Another approach, the using of electron beam physical vapor deposition (EB-PVD) method, produces coatings with columnar structures. It is well known that the columnar structure is excellent in thermal shock resistance and high temperature durability because of its excellent adaptability to deformation with the substrate [20-21]. However, coatings fabricated using EB-PVD have the disadvantage of a relatively high thermal conductivity, since the vertical fractures in the columnar structure are parallel to the direction of the heat flow [20-21].

Recently, the suspension plasma spray (SPS) method

*Corresponding author:
Tel : +82 31 645 1442
Fax: +86 31 645 1492
E-mail: ysoh30@kicet.re.kr

has been reported as an alternative to the previous methods [22-24]. This method fabricates a porous structure coating by spraying fine particles in a suspension [22-24]. Porosity is essential elements in the functionality of the thermal insulation coating influencing the thermal properties. [25]. The porous structure formed by the particles produces a coating that has low thermal conductivity and high thermal durability, which prevents excessive heating [10, 26]. In this study, Microstructure control and change in thermal conductivity of thermal insulation coating by suspension plasma spraying according to change in 8YSZ/SiO_2 particle sizes were investigated. Different milling method was used for grinding raw materials with different kinetic energy, and then, the grinding behaviors of raw materials according to each milling method were studied. The microstructural changes of SPS coatings according to the particle size of 8YSZ/ SiO_2 were investigated. Finally, thermal properties of coating according to the microstructural changes were studied.

Experimental Procedure

A disc-shaped Al and Si alloy substrate (Al 5052, Dong Yang Piston, Korea) with a diameter of 2.54 cm and thickness of 3 mm, was used as the coating substrate. In this study, the specimen was composed of a top coating, with a bond coating between the substrate and the top coating. First, the bond coating was fabricated using YSZ powder (8 mol% Y_2O_3-ZrO_2, 271-3, Praxair, USA). The top coating was prepared by mixing YSZ and SiO_2 powder (0.8 μm and 4 μm, Eq Solution, KOREA) with ratios of 7 : 3 and 5 : 5, followed by 24 hours of ball milling for YSZ and SiO_2 powder, 3 hours for YSZ powder, and 6 hours of planetary milling for SiO_2 powder to obtain a suspension. This suspension was used to fabricate the coating specimen, using the SPS method. The distance between the coating substrate and the plasma torch was 75 mm-80 mm, the slurry feed rate was 45 mL/min, the rotation speed of the specimen jig was 150 rpm, and the current was 220A for the coating process. Ar, He, and N_2 gases were used in the ratio of 75 : 15 : 10 for the gas composition during the plasma spraying. Table 1 shows the coating compositions and details of the process conditions.

Table 1. Information of coatings.

	Composition	Mixture ratio	Pretreatment
YSZ-SiO_2-1	YSZ/4μm- SiO_2	7:3	24 h ball mill
YSZ-SiO_2-2	YSZ/0.8μm- SiO_2	7:3	24 h ball mill
YSZ-SiO_2-3	YSZ/0.8μm- SiO_2	5:5	24 h ball mill
YSZ-SiO_2-4	YSZ/0.8μm- SiO_2	5:5	YSZ 6 h/SiO_2 3 h planetary mill

Before the coating process, the particle sizes of the raw material powder and suspension were analyzed using a laser scattering particle size distribution analyzer (LA-950V2, Horiba, Japan). For the coating specimen, X-ray diffraction (XRD, RINT-2500HF, Rigaku, Japan) was used to analyze the phase formation behavior by scanning for 20-80 ° and using the conditions of 40 kV, 200 mA, and a scan rate of 5 °/min. After polishing the cross section of the coating specimen using a diamond suspension to 1 μm, a scanning electron microscope (SEM, JSM-6770F, Jeol, Japan) was used to observe the microstructure of the coating layer, and the total porosity of coating layer was measured by the softwares ImageJ (ImaJ). The ratio of the areas of the pores in the areas of the coating layer from the SEM image was calculated to obtain porosity [27]. The apparent density of the coating was obtained by measuring its external dimensions after fabricating a free standing specimen. The specific heat of the coating was measured using a differential scanning calorimeter (DSC, DSC 204 F1, Netzsch, Germany) and the thermal diffusivity was measured by calculating the average value of 10 measurements with using a light flash apparatus (LFA, LFA 467 HT, Netzsch, Germany) at 25 ºC room temperature and 260 V laser flash.

Results and Discussions

Fig. 1 shows the particle size distribution of the raw material powder and the suspension used to coat the specimen. Fig. 1 shows results that are close to normal distributions, except for the 0.8 μm-SiO_2 series. Also, for the powders that underwent 24 hours of ball milling and planetary milling of 3 hours and 6 hours. The difference between the mean size and D_{50} was not significant. The mean size of the 0.8 μm SiO_2 decreased from 1.85 μm to 1.29 μm and the mean size of the 4 μm-SiO_2 decreased from 5.15 μm to 4.66 μm and the quantity of small peaks of the particle size distribution graph was increased. After 6 hours of planetary milling, the particle size of the YSZ decreased from 30.42 μm to 1.37 μm. After 3 hours of planetary milling, the particle size of the 0.8 μm SiO_2 decreased from 1.85 μm to 1.17 μm and the quantity of small peaks of the particle size graph was increased. It has been reported that the kinetic energy of planetary milling is greater than that of ball milling and, thus, it was assumed that the reduction would be greater after the planetary milling due to the difference in the kinetic energy [28]. The summary of particle size distribution of the raw material powder and the suspension used to coat the specimen are showed in Table 2.

The results of the X-ray diffraction analysis of the coated specimens are shown in Fig. 2. For all of the samples, a tetragonal phase YSZ and zircon (Zr-Si-O_4) were founded. It was previously reported that the (004)

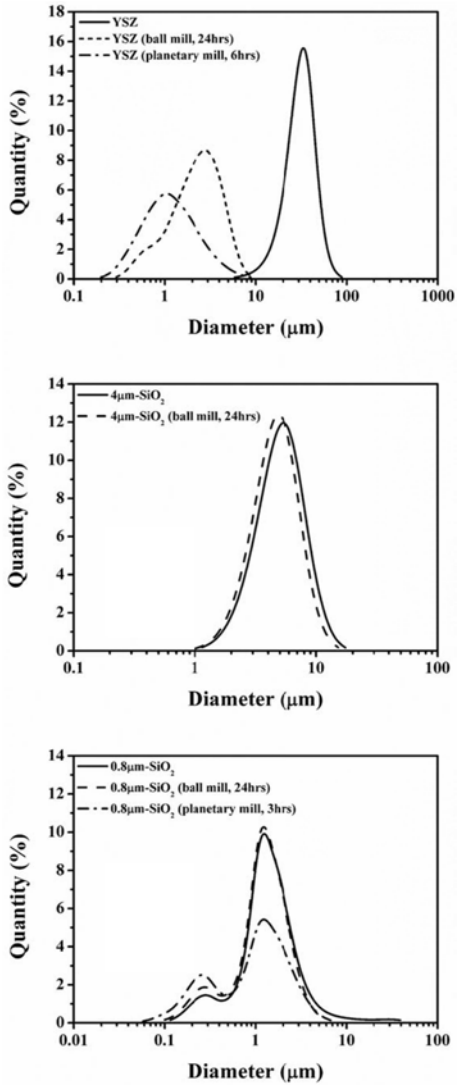

Fig. 1. Particle size of raw materials: YSZ, 4μm-SiO_2, 0.8 μm-SiO_2, YSZ (ball mill, 24 h), 4 μm-SiO_2 (ball mill, 24 h), 0.8 μm-SiO_2 (ball mill, 24 h), YSZ (planetary mill, 6 h), 0.8 μm SiO_2 (planetary mill, 3 h).

Table 2. Particle size of powders.

	D_{50} (μm)	Mean size (μm)
YSZ	29.54	30.42
YSZ (24h ball mill)	2.15	2.39
YSZ (6h planetary mill)	1.04	1.37
4μm-SiO_2	4.77	5.15
4μm-SiO_2 (24h ball mill)	4.34	4.66
0.8μm-SiO_2	1.26	1.85
0.8μm-SiO_2 (24h ball mill)	1.15	1.29
0.8μm-SiO_2 (3h planetary mill)	1.00	1.17

peak at 73 ° and (400) peak at 74 ° are observed for the tetragonal phase YSZ, while only the (400) peak at 2θ = 73.5 ° is observed for the hexagonal phase [29-30]. Also, it was reported that YSZ transforms into the metastable tetragonal phase ZrO_2 after the plasma

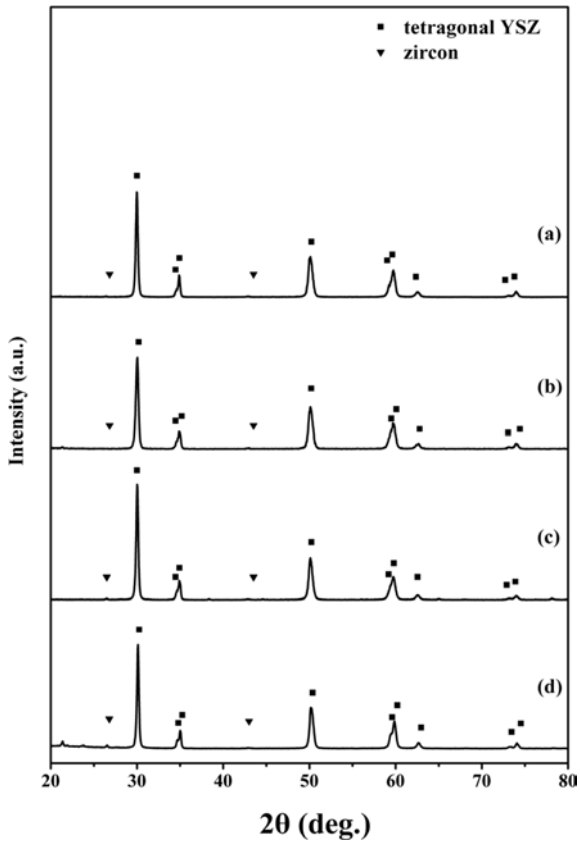

Fig. 2. X-ray diffraction patterns of coatings: (a) YSZ-SiO_2-1, (b) YSZ-SiO_2-2, (c) YSZ-SiO_2-3, (d) YSZ-SiO_2-4, (e) YSZ-SiO_2-5.

spray coating deposition and cooling [31-32]. In this study, the tetragonal phase was observed from the peaks at 73 ° and 74 ° of the coated specimen. Here, the effects of the particle sizes of the ingredients, and the mixing ratio were not significant.

The left side of Fig. 3 shows an image of the coating's cross sectional microstructure in SEM, and the right side shows the coated porous structure and the results of porosity analysis using the same SEM image. Fig. 3(a) shows the microstructure of the YSZ-SiO_2-1 fabricated following 24 hours of ball milling after mixing YSZ and 4 μm-SiO_2 with a 75 : 15 : 15 ratio composition of Ar, H_2, and N_2 gases. The bright area is the coating layer and the dark area on the left side is the mounting material. For this coating layer, a dense structure of 1.3% porosity was observed. Fig. 3(b) shows the microstructure of the YSZ-SiO_2-2 fabricated using the YSZ-SiO_2-1 processing conditions. 0.8 μm-SiO_2 (ball mill, 24 h) was used for the SiO_2 in the mixture and the other conditions were the same. For this coating layer, the porosity was 27.4%, which was significantly increased compared to YSZ-SiO_2-1. Based on this result, it was determined that the coating smaller increased with the finer particles of 0.8 μm-SiO_2 (ball mill, 24 h). It is assumed that particles having sizes below 1 μm did not have enough kinetic energy to reach the substrate when sprayed during the

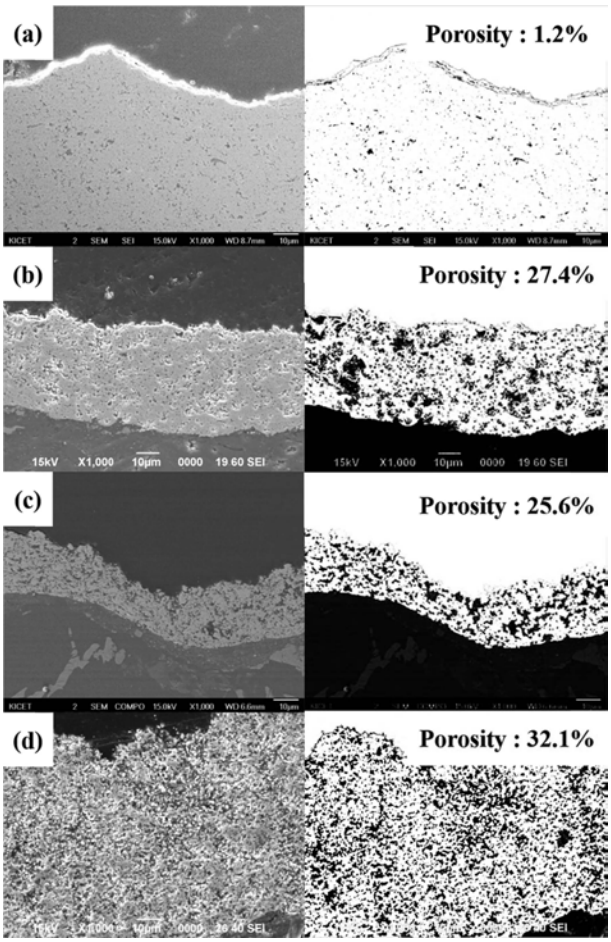

Fig. 3. SEM Images & Image analyzing of coatings: (a) YSZ-SiO_2-1, (b) YSZ-SiO_2-2, (c) YSZ-SiO_2-3, (d) YSZ-SiO_2-4, (e) YSZ-SiO_2-5.

suspension plasma coating process of above condition and porosity of the coating was increased [33-34]. Fig. 3(c) shows the microstructure image of YSZ-SiO_2-3, when the YSZ and 0.8 μm-SiO_2 mixing ratio was changed from 7 : 3 to 5 : 5. The YSZ-SiO_2-2 processing conditions were used, and all other conditions remained the same. The porosity of the coating layer was 25.6% and the porosity did not change significantly when the 0.8 μm-SiO_2 mixing ratio was increased. Fig. 3(d) shows the microstructure of the YSZ-SiO_2-4 sample. This was prepared after 6 hours and 3 hours of planetary milling for the YSZ powder and the SiO_2 powder, respectively, rather than the 24 hours ball milling of the YSZ and SiO_2 mixed suspension from the YSZ-SiO_2-3 processing conditions to reduce the overall particle size. The other conditions remained unchanged. Since the YSZ particle size was much larger than that of the SiO_2, the planetary milling of the YSZ was carried out for longer compared to the SiO_2. For this coating layer, it was found that the porosity was 32.1%, the highest among the cases. Based on the obtained results, it was determined that the distribution

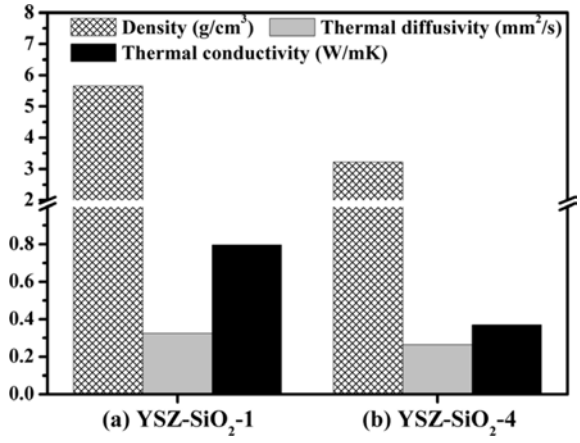

Fig. 4. Densities, thermal diffusivities, and thermal conductivities of coatings: (a) YSZ-SiO_2-1, (b) YSZ-SiO_2-4

of particles smaller than 1 μm in the particle size distribution of the 0.8 μm-SiO_2 (planetary mill, 3 h) increased, compared to that of the 0.8μm-SiO_2 (ball mill, 24 h), resulting in an increase in porosity. Also, the pore size was smaller and more evenly distributed, compared to the microstructures of YSZ-SiO_2-2 and YSZ-SiO_2-3. This was thought to be the result of the overall decrease in particle size.

The coating density, thermal diffusivity which are necessary into determining the thermal conductivity of the coating, and thermal conductivity measurement results for the coating were presented in Fig. 4. In order to evaluate the effect of the porosity on thermal conductivity, comparisons were made between YSZ-SiO_2-1 with the lowest porosity, and YSZ-SiO_2-4 with the highest porosity because porosity, it is widely known, has a strong impact on thermal conductivity of thermal insulation coating [25]. This comparison revealed that the apparent density of YSZ-SiO_2-1 in Fig. 4(a) was 5.662 g/cm^3 and the apparent density of YSZ-SiO_2-4 in Fig. 4(b) was 3.227 g/cm^3. The lower density for Fig. 4(b) YSZ-SiO_2-4 was thought to be a result of the higher porosity. The specific heats of YSZ-SiO_2-1 and YSZ-SiO_2-4 were measured to be about 0.433 J/(gK). Also, the thermal diffusivity of YSZ-SiO_2-1 in Fig. 4(a) was 0.317 mm^2/s, while the thermal diffusivity of YSZ-SiO_2-4 in Fig. 4(b) was 0.264 mm^2/s. Afterwards, the thermal conductivity of the coating was calculated using Eq. (1), as shown below [11, 23-24, 35].

$$\kappa = \rho \cdot C_p \cdot D \quad (1)$$

The coating thermal conductivity of YSZ-SiO_2-1 in Fig. 4(a) was calculated to be 0.797 and the coating thermal conductivity of YSZ-SiO_2-4 in Fig. 4(b) was calculated to be 0.369, revealing a decreasing trend in thermal conductivity when the porosity increased.

Conclusions

The particle sizes of the ingredients and their composition ratios were varied for the fabrication of 8YSZ/SiO_2 insulation coatings, using the suspension plasma spray (SPS) method. This was used to investigate the changes in the microstructure of the coating layer and the phase formation behavior, and to observe the variations in the thermal conductivities of specimens with different microstructures. The following conclusions were drawn in this study.

(1) The effects of the particle sizes of the ingredient, and the variations in the mixing ratios, on the microstructure formed by the suspension plasma coating, were observed. The changes in composition due to changes in the ingredient's mixing ratios had almost no impact on the porosity. However, when the particle sizes of the ingredients were varied, the porosity was found to change from 1.2% to 32.1%. This result showed that the particle sizes of the ingredient materials had a significant effect on the microstructure in SPS.

(2) The phase formation behavior of the coating in all the cases produced tetragonal zirconia and zircon was found. Here, the effects of the particle sizes of the ingredients, and the mixing ratio were not significant.

(3) Comparison of the thermal conductivities of the two coatings with the largest difference in porosity showed that a large difference in the thermal conductivities. The increase in coating porosity was found to cause a significant decrease in density and thermal diffusivity, and consequently reduced the thermal conductivity.

Acknowledgments

This work was supported by the Korea Institute of Ceramic Engineering and Technology, funded by the Industrial Strategic Technology Development Program (#10077479) of the Ministry of Trade, Industry and Energy (MOTIE).

References

1. A. Uzun, I. C¸ evik, and M. Akc¸il, Surface & Coatings Technology 116-119 (1999) 505-507.
2. I. Taymaz, K. C¸ akVr, and A. Mimaroglu, Surface & Coatings Technology 200 (2005) 1182-1185.
3. E. Bu¨yu¨kkaya, T. Engin, and M. Cerit, Energy Conversion and Management 47 (2006) 1298-1310.
4. J. Vetter, G. Barbezat, J. Crummenauer, and J. Avissar, Surface & Coatings Technology 200 (2005) 1962-1968
5. Th. Lampe, S. Eisenberg, and E. Rodr´ıguez Cabeo, Surface & Coatings Technology 174-175 (2003) 1-7.
6. I.I. Taymaz, Surface & Coatings Technology 201 (2007) 5249-5252.
7. T. Hejwowski, and A. Weronski, Vacuum 65 (2002) 427-432.
8. M.R. Loghman-Estarki, R. Shoja Razavi, H. Edris, S.R. Bakhshi, M. Nejati, and H. Jamali, Ceramics International 42 (2016) 7432-7439.
9. E. Buyukkaya, and M. Cerit, Surface & Coatings Technology 202 (2007) 398-402.
10. N.P. Padture, M. Gell, E.H. Jordan, Science 296 (2002) 280-284.
11. S.K. Rupangudi, C.S. Ramesh, K. Veerabhadhrappa, R.R. V, SAE International Journal of Materials and Manufacturing 7[3] (2014) 633-637.
12. Th. Lampe, S. Eisenberg, and E. Rodr´ıguez Cabeo, Surface & Coatings Technology 174-175 (2003) 1-7.
13. G. Zhang, X. Fan, R. Xu, L. Su, and T.J. Wang, Ceramics International 44 (2018) 12655-12663.
14. A.G. Evans, D.R. Clarke, and C.G. Levi, Journal of the European Ceramic Society 28 (2008) 1405-1419.
15. A.G. Evans, D.R. Mumm, J.W. Hutchinson, G.H. Meier, and F.S. Pettit, Progress in Materials Science 46 (2001) 505-533.
16. B.-K. Jang, and H. Matsubara, Journal of the European Ceramic Society, 26 (2006) 1585-1590.
17. K.S. Ravichandran, K. An, R.E. Dutton, and S.L. Semiatin, J. Am. Ceram. Soc. 82 (1999) 673.
18. A. Rabiei and A.G. Evans, Acta Mater. 48 (2000) 3963-3976.
19. F. Zhou, Y. Wang, Z. Cui, L. Wang, J. Gou, Q. Zhang, and C. Wang, Ceramics International 43 (2017) 4102-4111.
20. H.B. Guo, S. Kuroda, and H. Murakami, J. Am. Ceram. Soc. 89 (2006) 1432-1439.
21. X.F. Zhang, K.S. Zhou, M. Liu, C.M. Deng, C.G. Deng, J.B. Song, and X. Tong, Ceramics International 42 (2016) 13969-13975.
22. K. Van Every, M.J.M. Krane, R.W. Trice, H. Wang, W. Porter, M. Besser, and D. Sordelet, J. Therm. Spray. Technol. 20 (2011) 817-828.
23. A. Guignard, G. Mauer, R. Vaßen, and Detlev Sto¨ver, J. Therm. Spray Technol. 21 (2012) 416-424.
24. H. Kassner, R. Siegert, D. Hathiramani, R. Vassen, and Detlev Stoever, J. Therm. Spray Technol. 17 (2007) 115-123.
25. B. Roge´, A. Fahr, J.S.R. Gigue` re, and K.I. McRae, ASM International 12[4] (2003) 530-535.
26. R. Ghasemi, and H. Vakilifard, Ceramics International, 43 (2017) 8556-8563.
27. S. Passoni, F. da S. Borges, L. F. Pires, S. da C. Saab, M. Cooper, Ciênc. agrotec. 38 [2] (2014) 122-128.
28. M. Abdellaoui, and E. Gaffet, Acta metallurgica et Materialia 43 (1994) 1087-1098.
29. N. Markocsan, P. Nylén, J. Wigren, and X.H. Li, Journal of Thermal Spray Technology 16 (2007) 498-505.
30. R. Srinivasan, R.J. De Angelis, G. Ice, and B.H. Davis, Journal of Materials Research 6 (2011) 1287-1292.
31. M. Rahaman, J. Gross, R. Dutton, and H. Wang, Acta Materialia 54 (2006) 1615-1621.
32. J. Feng, B. Xiao, R. Zhou, and W. Pan, Scripta Materialia 68 (2013) 727-730.
33. S. Wall, W. John, H.-c. Wang, and S.L. Goren, Aerosol Science and Technology 12[4] (1990) 926-946.
34. J. Laskin, and C. Lifshitz, JOURNAL OF MASS SPECTROMETRY 36 (2001) 459-478.
35. K. VanEvery, M.J.M. Krane, R.W. Trice, H. Wang, W. Porter, M. Besser, D. Sordelet, J. Ilavsky, and J. Almer, Journal of Thermal Spray Technology 20 (2011) 817-828.